



Supplement of

Comparison of airborne measurements of NO, NO₂, HONO, NO_y, and CO during FIREX-AQ

Ilann Bourgeois et al.

Correspondence to: Ilann Bourgeois (ilannbourgeois@hotmail.com) and Jeff Peischl (jeff.peischl@noaa.gov)

The copyright of individual parts of the supplement might differ from the article licence.

S1. Characterization of aerosol transmission in the CL instrument NO_y inlet

Agreement within stated uncertainties between total NO_y measured by CL and ΣNO_y (Figure 9), where pNO₃ (including both inorganic and organic fractions) was often a major contributor (Figure 10), suggests that most, if not all, of the pNO₃ mass measured by the AMS instrument is sampled and converted into NO by the CL instrument NO_y channel. However, potential particle losses can occur in several places of the NO_y inlet of the CL instrument. The NO_y inlet, extensively described by Ryerson et al. (1999), consists of a straight, heated assembly mounted perpendicularly to the flight direction of the aircraft. Sampling of ambient air occurs under constant mass flow conditions (1029.5 ± 0.2 sccm) through a sub-critical orifice 1.0 mm in diameter. Sampled air flows through a heated (90°C) CTFE manifold into a heated (300°C) gold tube catalyst that volatilizes and catalytically converts NO_y species, including pNO₃, to NO, which is then analyzed by the CL instrument. Here, we define particle losses as those particles that are sampled by the AMS but not by the NO_y CL channel as NO. Particle losses may occur in several places:

1. At the entry of the NO_y inlet (due to aspiration losses at a 90° angle).
2. In the CTFE manifold and in the gold tube catalyst by diffusion/impaction.
3. In the CTFE manifold by electrostatic deposition of small particles, due to possible build-up of charges on the non-conductive surface.
4. In the gold tube catalyst due to incomplete evaporation of the particle or incomplete conversion of pNO₃ into NO.

Outside of urban plumes pNO₃ is typically well mixed with the bulk of the accumulation mode (e.g., DeCarlo et al., 2008). Therefore, the volatility observed for ambient pNO₃ is typically close to the bulk volatility (Huffman et al., 2009). Ammonium nitrate is very volatile and evaporates at ~200°C (Docherty et al., 2015). Clarke (1991) reported that in a denuder tube with a residence time of ~0.35 seconds all non-refractory particulate species except ammonium sulfate (hence including pNO₃) evaporated at 150°C while ammonium sulfate evaporated at 300°C. Since the residence time in that study is comparable to the residence time in the NO_y inlet at lower aircraft altitudes (Figure S1 right panel), pNO₃ should be fully volatilized in the gold catalyst of the NO_y inlet heated at 300°C. Note that more refractory inorganic nitrate salts such as sodium nitrate (often associated with sea salt) and calcium nitrate (from dust) are not considered here, but these are normally associated with supermicron-sized particles and unlikely to be sampled by the NO_y inlet, as discussed in the next section.

To further characterize pNO₃ physical losses listed above, a multistage flow model of the NO_y inlet was constructed following the template of the Particle Loss Calculator (von der Weiden et al., 2009). The model calculates all aerodynamic particle losses at each stage of the NO_y inlet and provides an estimate of the total pNO₃ sampling efficiency. We used the US Standard Atmosphere and the NASA DC-8 cruise speeds as the ambient boundary conditions, as previously described by Guo et al. (2021).

Aerodynamic performance of the NO_y inlet

The main sources of aerodynamic particle loss in the NO_y inlet are the aspiration losses into the 1.0 mm orifice at the tip of the inlet (Figure S1 left panel). However, calculated aspiration losses come with large uncertainties for several reasons:

- Aspiration losses at a certain angle are calculated with equations designed for a thin tube sampling at moderate (5–20 m s⁻¹) air speeds (Hangal and Willeke, 1990; Li and Lundgren, 2002). Extrapolating these findings to FIREX-AQ-typical air speeds of 150–250 m s⁻¹ results in large uncertainty. Tsai et al. (1995) have investigated particle losses in thick-walled samplers, but their work predicts even larger, likely unrealistic losses when extrapolated to high air speeds (Figure S1 left panel).
- There is to the best of our knowledge no other theoretical estimation of aerosol losses for this type of inlet geometry. However, black carbon sampling efficiency was recently tested on a fairly similar inlet to that of the CL instrument (Perring et al., 2013). Unfortunately, no computational fluid dynamics modeling was performed in that study. The authors empirically demonstrated that their inlet quantitatively sampled aerosol accumulation mode in the upper troposphere (UT), probably up to 500 nm (see Brock et al., 2021 for typical aerosol size distributions in the UT). The authors reported clear losses for cloud particles larger than 1 μm, which may be considered by analogy as an upper transmission boundary for the NO_y inlet. Note that while the overall inlet geometry used in that study was very similar to that of the NO_y inlet, the tip orifice diameter was larger and the sampled air speed was lower. Hence, these results may not be directly transferrable to the NO_y inlet. Using the Hangal & Willeke (1990) equations, we calculate a ~450 nm cutoff for aerosol transmission by the Perring et al. (2013) inlet. This suggests that while model calculations are likely too conservative at high air speeds, they still have some predictive value.
- Both the inlet described by Perring et al. (2013) and the NO_y inlet were equipped with a flat and perpendicular flow plate mounted at the tip of the inlet to shield the inlet flow from turbulence caused by the inlet pylon. In the case of the NO_y inlet with its smaller sampling orifice, air may have been sampled from inside the boundary layer of the flow plate. This may have resulted in a lower air speed at the tip of the NO_y inlet than the aircraft speed. We investigated the uncertainty of our model by considering the effect of different air speeds on aerosol transmission in the NO_y inlet.

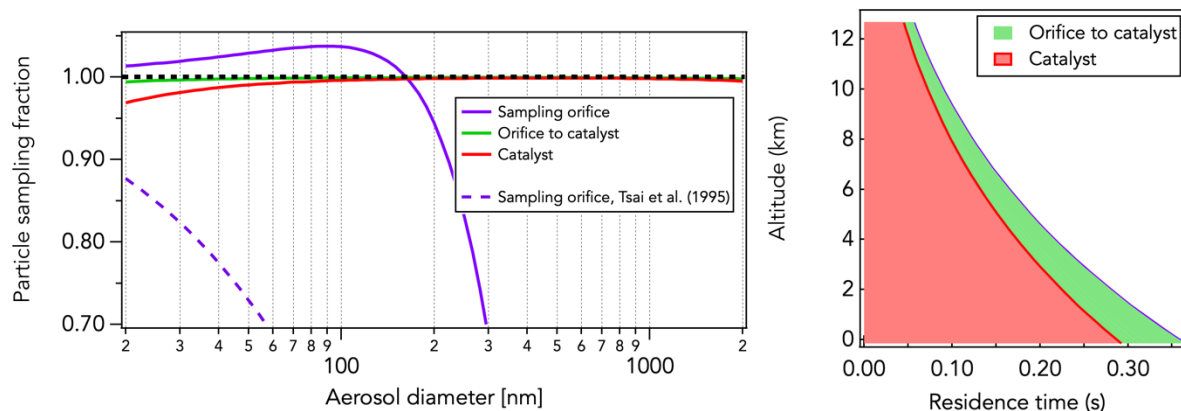


Figure S1 Left: Aerosol losses/enhancements calculated for each stage of the NO_y inlet at 5 km in altitude and for a sampled air speed 65% that of the typical NASA DC-8 cruising speed. Also shown is the particle sampling fraction calculated using the approach formulated by Tsai et al. (1995). Right: Residence time in the NO_y inlet, from the tip to the beginning of the gold catalyst (green) and in the catalyst itself (red). Note that the model assumes that full volatilization of pNO_3 only occurs at the end of the catalyst, thus overestimating diffusion losses.

Estimation of particle losses and sensitivity to air speed

The model was run using three different sampled air speeds: 40%, 65% and 100% of the aircraft speed. The computed losses were then applied to a case study of the Williams Flat fire smoke sampled on 07/08/2019 in which pNO_3 concentrations were large and variable and pNO_3 mass size distributions were measured. The calculated pNO_3 fraction not sampled through the NO_y inlet ranged from 20 to 90%, emphasizing the model sensitivity to sampled air speed. The top three panels in Figure S2 show the correlation between $\Delta\text{NO}_{y\text{Sum-CL}}$ and the modeled pNO_3 not sampled through the NO_y inlet using three different sampled air speeds. The bottom three panels in Figure S2 show the correlation between $\Delta\text{NO}_{y\text{Sum-CL}}$ and the modeled pNO_3 not sampled through the NO_y inlet after removing the calculated pNO_3 losses from ΣNO_y . An assumed air speed of 65% that of the aircraft yields the lowest residuals between $\Delta\text{NO}_{y\text{Sum-CL}}$ and the modeled pNO_3 losses, suggesting that it may be a good approximation of the sampled air speed in the NO_y inlet.

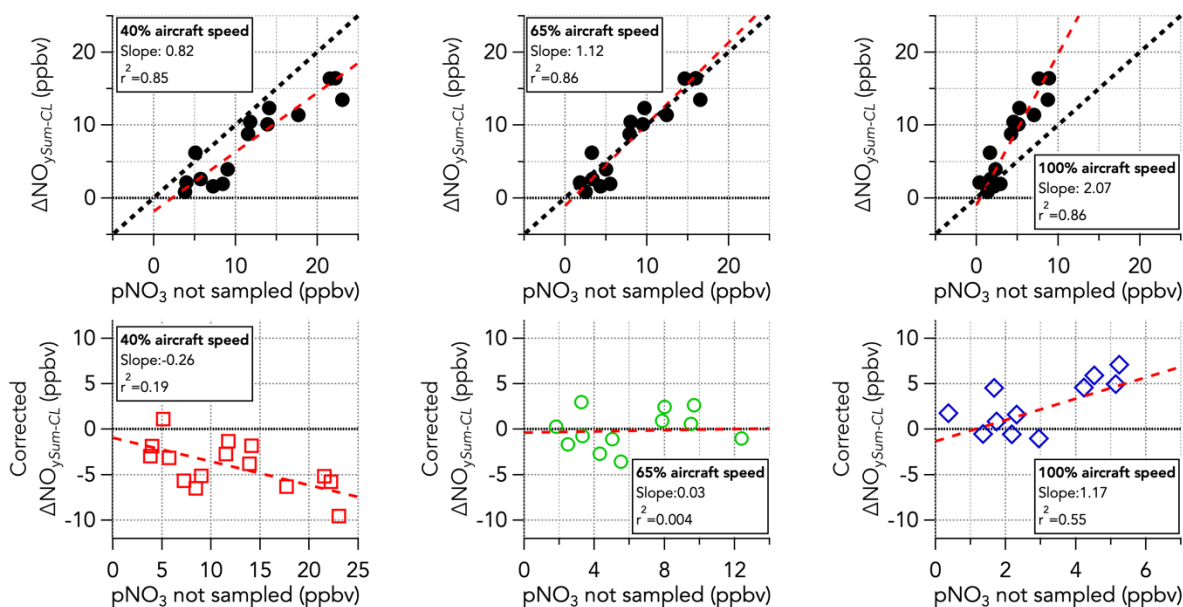


Figure S2 The top three panels show the correlation between $\Delta\text{NO}_{y\text{Sum-CL}}$ and the modeled pNO_3 not sampled through the NO_y inlet for an assumed sampled air speed of 100% (left), 65% (middle) and 40% (right) that of the aircraft for several Williams Flat fire (WFF) smoke plume transects on 07/08/2019. Each marker corresponds to the average value for one individual smoke plume transect. The bottom three panels show the correlation between $\Delta\text{NO}_{y\text{Sum-CL}}$ and the modeled pNO_3 not sampled through the NO_y inlet after removing the calculated pNO_3 losses from ΣNO_y .

So far, we have used the HR-AMS (see section 2.2.8 of the main text) pNO_3 mass size distributions to estimate pNO_3 losses in the NO_y inlet. During FIREX-AQ, bulk aerosol volume size distributions were measured with a Laser Aerosol Spectrometer (LAS) and were overall comparable to measured distributions by the HR-AMS (Moore et al., 2021). However, some discrepancies were observed in dense smoke. The sensitivity of pNO_3 sampling fraction to the pNO_3 mass size distributions as measured by the HR-AMS and LAS instruments is shown in Figure S3. At a typical FIREX-AQ sampling altitude of 4–5 km, the uncertainty in the pNO_3 mass size distribution adds an additional $\sim 10\%$ uncertainty to the pNO_3 sampling fraction through the NO_y inlet.

Figure 12a shows the overall calculated altitude and size dependence of pNO_3 pNO_3 sampling fraction through the NO_y inlet (assuming a sampled air speed 65% that of the aircraft). pNO_3 mass size distribution in the accumulation mode is weighted towards larger sizes in fresh fire smoke, resulting in a calculated pNO_3 sampling fraction through the NO_y inlet of about 50%. For remote and lightly polluted conditions, typical aerosol accumulation mode sizes are considerably smaller. For instance, about 85% of pNO_3 would have been sampled by the NO_y inlet for the range of conditions found over Seoul, South Korea (Nault et al., 2018) according to the model.

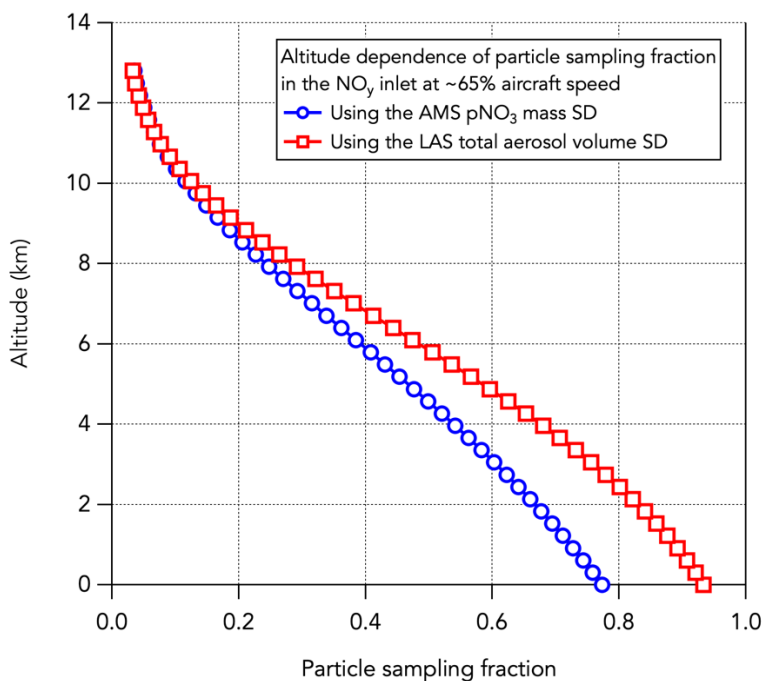


Figure S3 Comparison of the calculated pNO₃ mass fraction sampled by the NO_y inlet assuming a sampled air speed 65% that of the aircraft and using either the average pNO₃ mass size distribution (SD) measured by HR-AMS (blue) or the average pNO₃ volume size distribution measured by LAS (red) in fire smoke on 07/08/2019. Note that ambient size distributions are not constant with altitude, so these are simplified estimations.

In addition to the aspiration losses there exist diffusion losses of small particles (<100 nm) in the NO_y inlet (Figure S1). These diffusion losses are mostly independent of altitude and may be overestimated as small particles are assumed in the model to be volatilized at the end of the gold catalyst. Another source of loss in this size range is electrostatic deposition of aerosols on the surface of the CTFE manifold. As reported in Kenagy et al. (submitted), these losses are dependent on charge polarity and residence time. Extrapolation of the laboratory calibrations done by Kenagy et al. (submitted) resulted in less than 5% loss of sub-100 nm particles in the NO_y inlet.

References:

Brock, C. A., Froyd, K. D., Dollner, M., Williamson, C. J., Schill, G., Murphy, D. M., Wagner, N. J., Kupc, A., Jimenez, J. L., Campuzano-Jost, P., Nault, B. A., Schroder, J. C., Day, D. A., Price, D. J., Weinzierl, B., Schwarz, J. P., Katich, J. M., Wang, S., Zeng, L., Weber, R., Dibb, J., Scheuer, E., Diskin, G. S., DiGangi, J. P., Bui, T., Dean-Day, J. M., Thompson, C. R., Peischl, J., Ryerson, T. B., Bourgeois, I., Daube, B. C., Commane, R., and Wofsy, S. C.: Ambient aerosol properties in the remote atmosphere from global-scale in situ measurements, *Atmospheric Chem. Phys.*, 21, 15023–15063, <https://doi.org/10.5194/acp-21-15023-2021>, 2021.

Clarke, A. D.: A thermo-optic technique for in situ analysis of size-resolved aerosol physicochemistry, *Atmospheric Environ. Part Gen. Top.*, 25, 635–644, [https://doi.org/10.1016/0960-1686\(91\)90061-B](https://doi.org/10.1016/0960-1686(91)90061-B), 1991.

Crouse, J. D., McKinney, K. A., Kwan, A. J., and Wennberg, P. O.: Measurement of Gas-Phase Hydroperoxides by Chemical Ionization Mass Spectrometry, *Anal. Chem.*, 78, 6726–6732, <https://doi.org/10.1021/ac0604235>, 2006.

Crouse, J. D., DeCarlo, P. F., Blake, D. R., Emmons, L. K., Campos, T. L., Apel, E. C., Clarke, A. D., Weinheimer, A. J., McCabe, D. C., Yokelson, R. J., Jimenez, J. L., and Wennberg, P. O.: Biomass burning and urban air pollution over the Central Mexican Plateau, *Atmos Chem Phys*, 16, 2009.

DeCarlo, P. F., Dunlea, E. J., Kimmel, J. R., Aiken, A. C., Sueper, D., Crouse, J., Wennberg, P. O., Emmons, L., Shinozuka, Y., Clarke, A., Zhou, J., Tomlinson, J., Collins, D. R., Knapp, D., Weinheimer, A. J., Montzka, D. D., Campos, T., and Jimenez, J. L.: Fast airborne aerosol size and chemistry measurements above Mexico City and Central Mexico during the MILAGRO campaign, *Atmospheric Chem. Phys.*, 8, 4027–4048, <https://doi.org/10.5194/acp-8-4027-2008>, 2008.

Docherty, K. S., Lewandowski, M., and Jimenez, J. L.: Effect of Vaporizer Temperature on Ambient Non-Refractory Submicron Aerosol Composition and Mass Spectra Measured by the Aerosol Mass Spectrometer, *Aerosol Sci. Technol.*, 49, 485–494, <https://doi.org/10.1080/02786826.2015.1042100>, 2015.

Guo, H., Campuzano-Jost, P., Nault, B. A., Day, D. A., Schroder, J. C., Kim, D., Dibb, J. E., Dollner, M., Weinzierl, B., and Jimenez, J. L.: The importance of size ranges in aerosol instrument intercomparisons: a case study for the Atmospheric Tomography Mission, *Atmospheric Meas. Tech.*, 14, 3631–3655, <https://doi.org/10.5194/amt-14-3631-2021>, 2021.

Hangal, S. and Willeke, K.: Overall efficiency of tubular inlets sampling at 0–90 degrees from horizontal aerosol flows, *Atmospheric Environ. Part Gen. Top.*, 24, 2379–2386, [https://doi.org/10.1016/0960-1686\(90\)90330-P](https://doi.org/10.1016/0960-1686(90)90330-P), 1990.

Huffman, J. A., Docherty, K. S., Aiken, A. C., Cubison, M. J., Ulbrich, I. M., DeCarlo, P. F., Sueper, D., Jayne, J. T., Worsnop, D. R., Ziemann, P. J., and Jimenez, J. L.: Chemically-resolved aerosol volatility measurements from two megacity field studies, *Atmospheric Chem. Phys.*, 9, 7161–7182, <https://doi.org/10.5194/acp-9-7161-2009>, 2009.

Li, S.-N. and Lundgren, D. A.: Aerosol Aspiration Efficiency of Blunt and Thin-Walled Samplers at Different Wind Orientations, *Aerosol Sci. Technol.*, 36, 342–350, <https://doi.org/10.1080/027868202753504533>, 2002.

Moore, R. H., Wiggins, E. B., Ahern, A. T., Zimmerman, S., Montgomery, L., Campuzano Jost, P., Robinson, C. E., Ziemba, L. D., Winstead, E. L., Anderson, B. E., Brock, C. A., Brown, M. D., Chen, G., Crosbie, E. C., Guo, H., Jimenez, J. L., Jordan, C. E., Lyu, M., Nault, B. A., Rothfuss, N. E., Sanchez, K. J., Schueneman, M., Shingler, T. J., Shook, M. A., Thornhill, K. L., Wagner, N. L., and Wang, J.: Sizing response of the Ultra-High Sensitivity Aerosol Spectrometer (UHSAS) and Laser Aerosol Spectrometer (LAS) to changes in submicron aerosol composition and refractive index, *Atmospheric Meas. Tech.*, 14, 4517–4542, <https://doi.org/10.5194/amt-14-4517-2021>, 2021.

Nault, B. A., Campuzano-Jost, P., Day, D. A., Schroder, J. C., Anderson, B., Beyersdorf, A. J., Blake, D. R., Brune, W. H., Choi, Y., Corr, C. A., de Gouw, J. A., Dibb, J., DiGangi, J. P., Diskin, G. S., Fried, A., Huey, L. G., Kim, M. J., Knote, C. J., Lamb, K. D., Lee, T., Park, T., Pusede, S. E., Scheuer, E., Thornhill, K. L., Woo, J.-H., and Jimenez, J. L.: Secondary organic aerosol production from local emissions dominates the organic aerosol budget over Seoul, South Korea, during KORUS-AQ, *Atmospheric Chem. Phys.*, 18, 17769–17800, <https://doi.org/10.5194/acp-18-17769-2018>, 2018.

Norman, M., Hansel, A., and Wisthaler, A.: O₂⁺ as reagent ion in the PTR-MS instrument: Detection of gas-phase ammonia, *Int. J. Mass Spectrom.*, 265, 382–387, <https://doi.org/10.1016/j.ijms.2007.06.010>, 2007.

Perring, A. E., Schwarz, J. P., Gao, R. S., Heymsfield, A. J., Schmitt, C. G., Schnaiter, M., and Fahey, D. W.: Evaluation of a Perpendicular Inlet for Airborne Sampling of Interstitial Submicron Black-Carbon Aerosol, *Aerosol Sci. Technol.*, 47, 1066–1072, <https://doi.org/10.1080/02786826.2013.821196>, 2013.

Ryerson, T. B., Huey, L. G., Knapp, K., Neuman, J. A., Parrish, D. D., Sueper, D. T., and Fehsenfeld, F. C.: Design and initial characterization of an inlet for gas-phase NO_y measurements from aircraft, *J. Geophys. Res. Atmospheres*, 104, 5483–5492, <https://doi.org/10.1029/1998JD100087>, 1999.

Tsai, P.-J., Vincent, J. H., Mark, D., and Maldonado, G.: Impaction Model for the Aspiration Efficiencies of Aerosol Samplers in Moving Air under Orientation-Averaged Conditions, *Aerosol Sci. Technol.*, 22, 271–286, <https://doi.org/10.1080/02786829408959746>, 1995.

von der Weiden, S.-L., Drewnick, F., and Borrmann, S.: Particle Loss Calculator – a new software tool for the assessment of the performance of aerosol inlet systems, *Atmospheric Meas. Tech.*, 2, 479–494, <https://doi.org/10.5194/amt-2-479-2009>, 2009.

S2. Supplementary Figures

	ALL DATA	SMOKE DATA
BASE	1.00	0.99
NO LIF	0.98	0.99
CES HONO	1.04	1.08
CES NO2	0.94	0.91

Table S1 Correlation slopes between the sum of individually measured NO_y species (= NO_x + HONO + HNO₃ + APNs + pNO₃) against the total NO_y measurement by CL Base case corresponds to using CL NO_x and CIMS HONO.

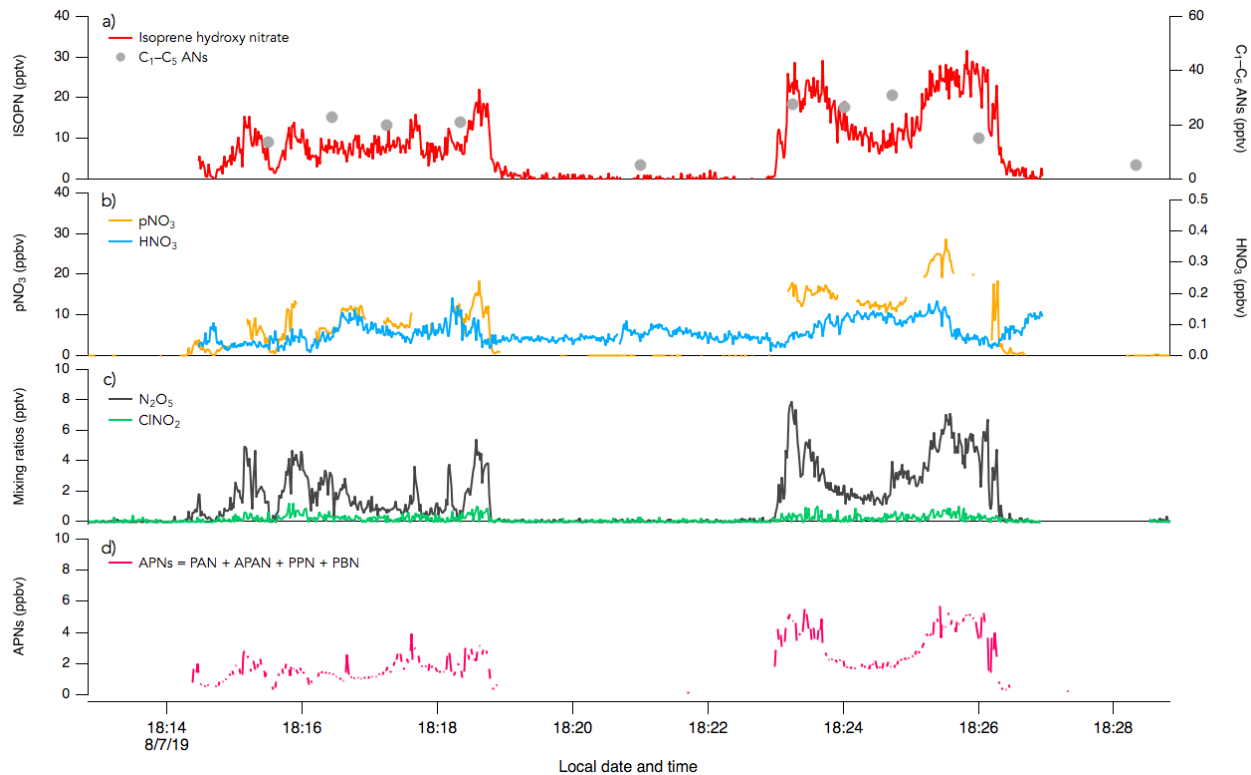


Figure S4 1 s measurements of a) Isoprene hydroxy nitrate (ISOPN) and C₁-C₅ alkyl nitrates (ANs), b) particulate nitrate (pNO₃) and HNO₃, c) N₂O₅ and ClNO₂ and d) APNs during two crosswind plume transects of smoke from the Williams Flat fire on 07/08/2019. The plume transects were chosen due to the significant enhancement of all species at that time.



Figure S5 1 s measurements of a) Isoprene hydroxy nitrate (ISOPN) and C₁-C₅ alkyl nitrates (ANs), b) particulate nitrate (pNO₃) and HNO₃, c) N₂O₅ and ClNO₂ and d) APNs during crosswind plume transects of smoke from crop burning in southeastern US on 30/08/2019.

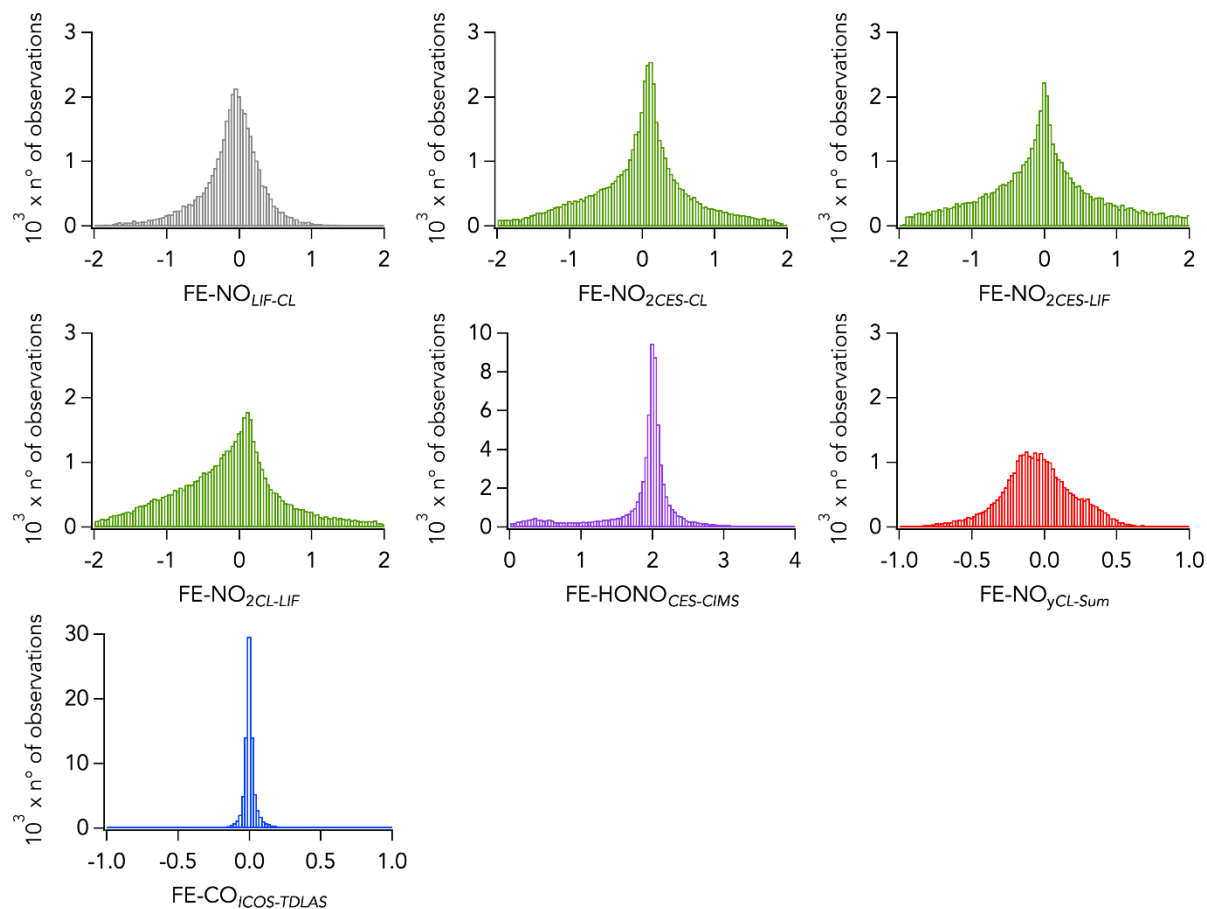


Figure S6 Histograms of the fractional error (FE) of 1 s measurements of NO (grey), NO₂ (green), HONO (purple), NO_y (red) and CO (blue) for all air parcels sampled in fire smoke. The tight distribution of FE-HONO_{CES-CIMS} around a value of 2 is due to the lower precision of the CES instrument when HONO mixing ratios were close to 0 (~90% of the data in smoke).

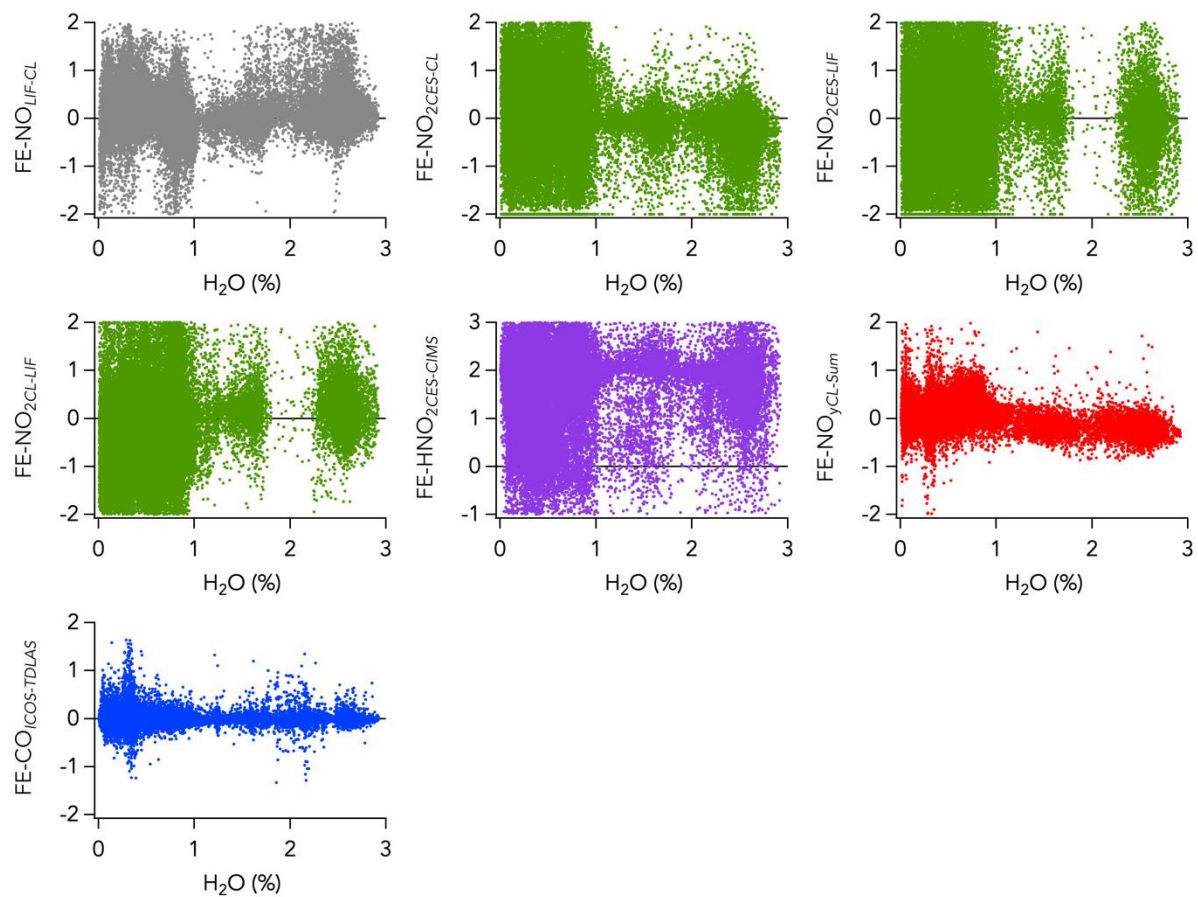


Figure S7 Fractional error (FE) of 1 s measurements of NO (grey), NO₂ (green), HONO (purple), NO_y (red) and CO (blue) as a function of water vapor for all air parcels sampled in fire smoke.

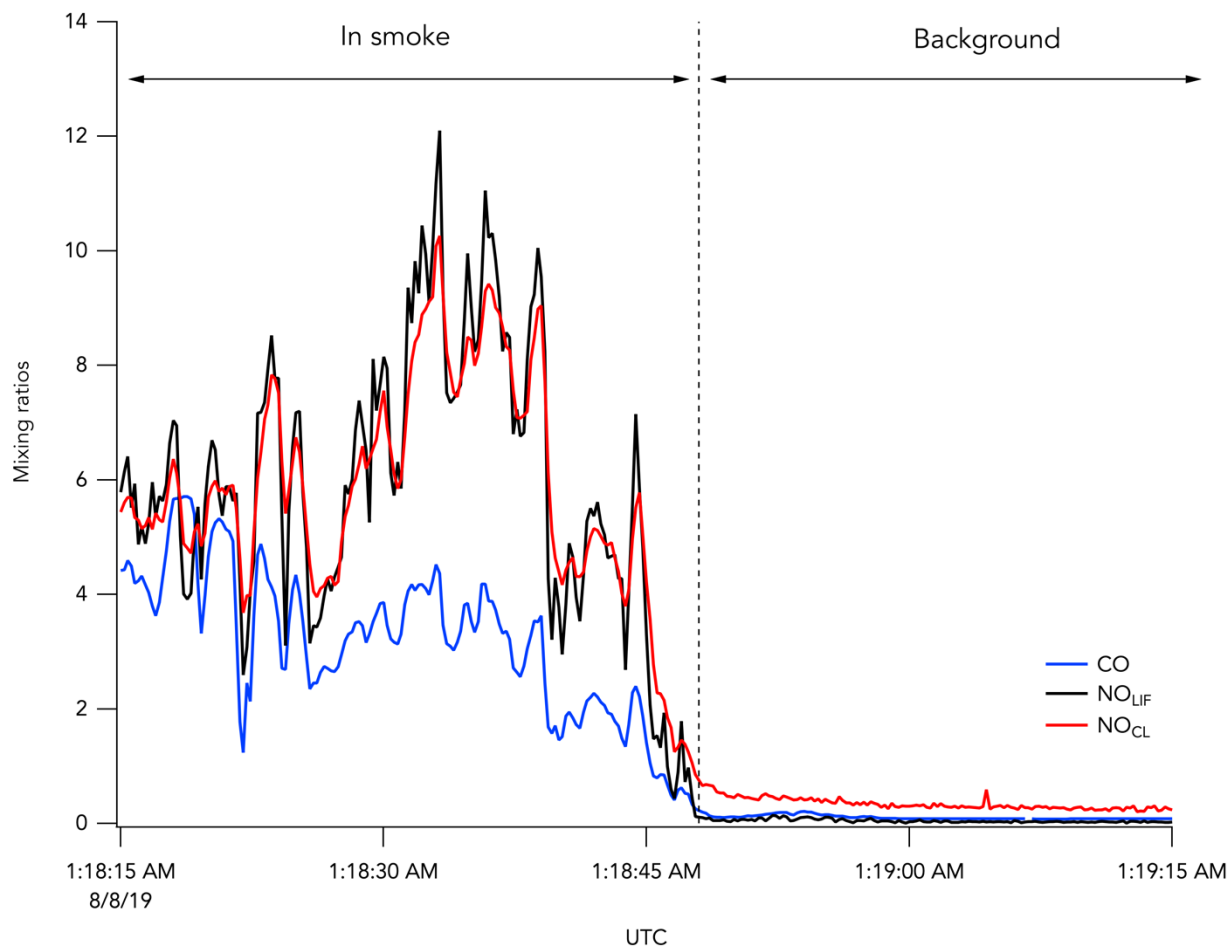


Figure S8 10Hz measurements of NO by LIF (black) and CL (red) and CO (blue) during the transition from smoke to background air during the Williams Flat fire on 07/8/2019.

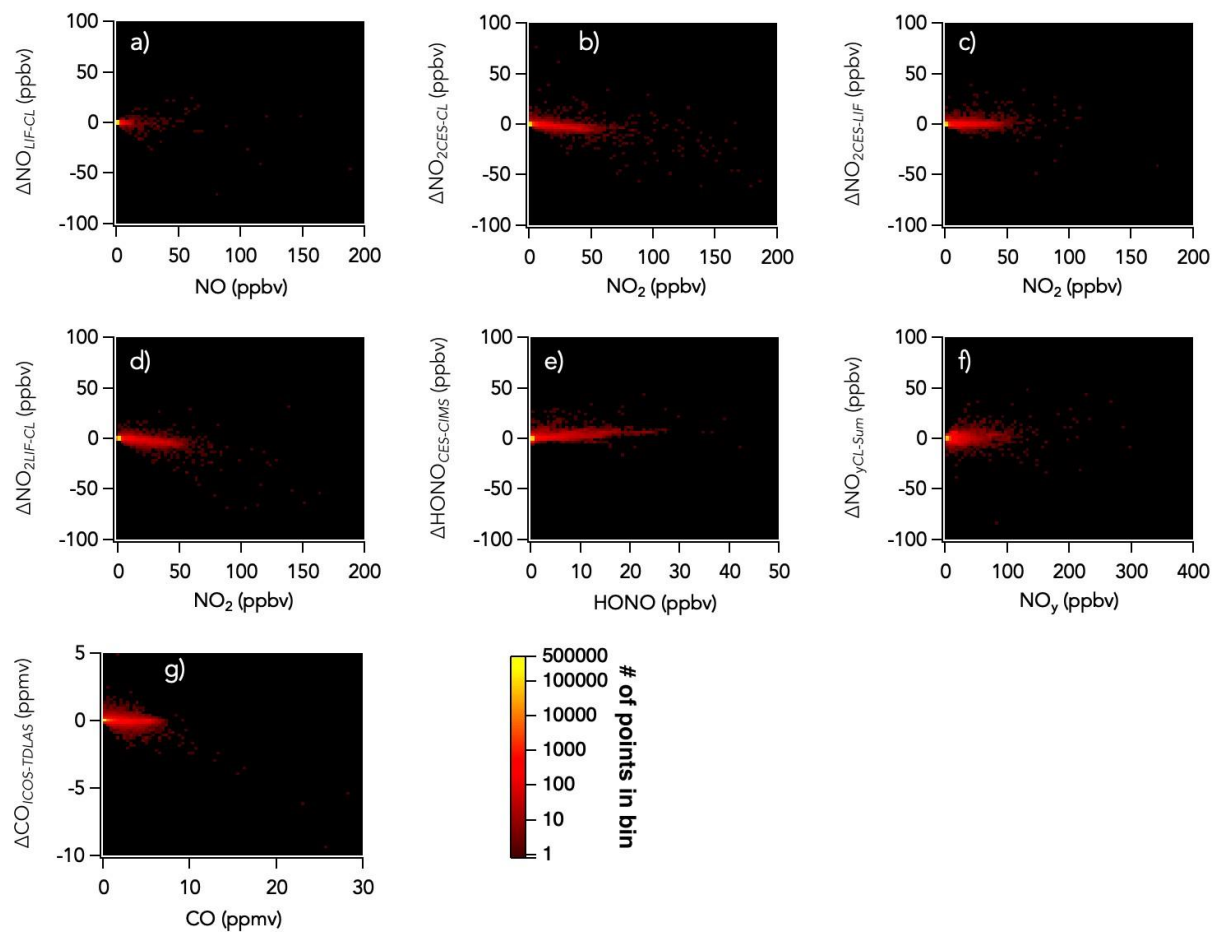


Figure S9 Measurement differences (1Hz data) of a) NO, b)–d) NO_2 , e) HONO, f) NO_y , g) CO as a function of the species mixing ratios for the entire campaign. The color bar (log scale) indicates the number of individual data points per bin of mixing ratios (bin size is 2.5×2.5 ppbv).

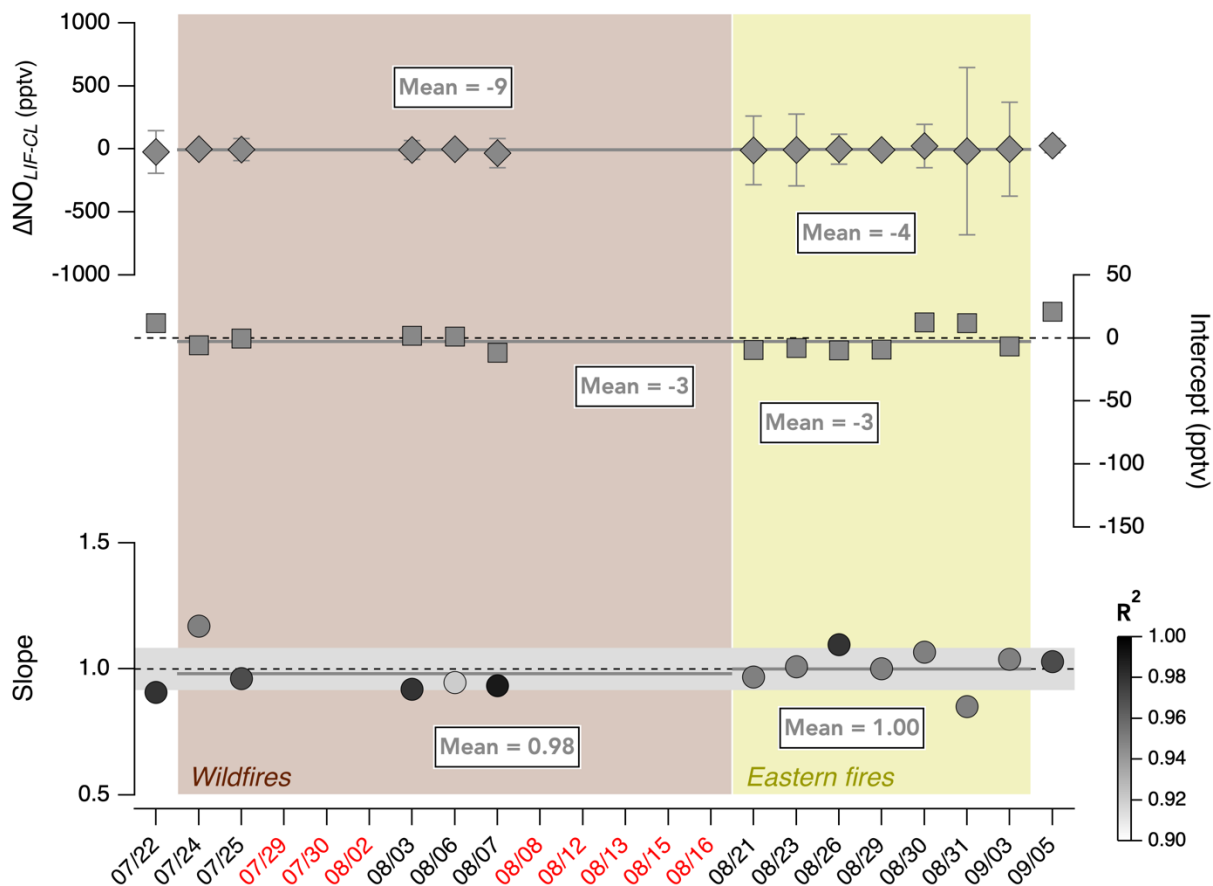


Figure S10 Individual flight comparison of 1Hz NO measurements by LIF versus CL. Slopes (circles) are reported in the bottom panel and colored by the correlation coefficient value as indicated by the color scale. Intercepts (grey squares) are reported in the middle panel, and mean $\Delta\text{NO}_{\text{LIF-CL}}$ (grey diamonds) values are reported in the top panel. The solid grey lines correspond to the average values of each parameter across all wildfire (brown shaded area) and eastern fire (yellow shaded area) flights. The first and last flights correspond to the LA Basin flights. The black dotted lines show the zero. The grey shaded area in the bottom panel indicates the propagated analytical uncertainty. Flight dates in red indicate that at least one instrument did not report data for those flights.

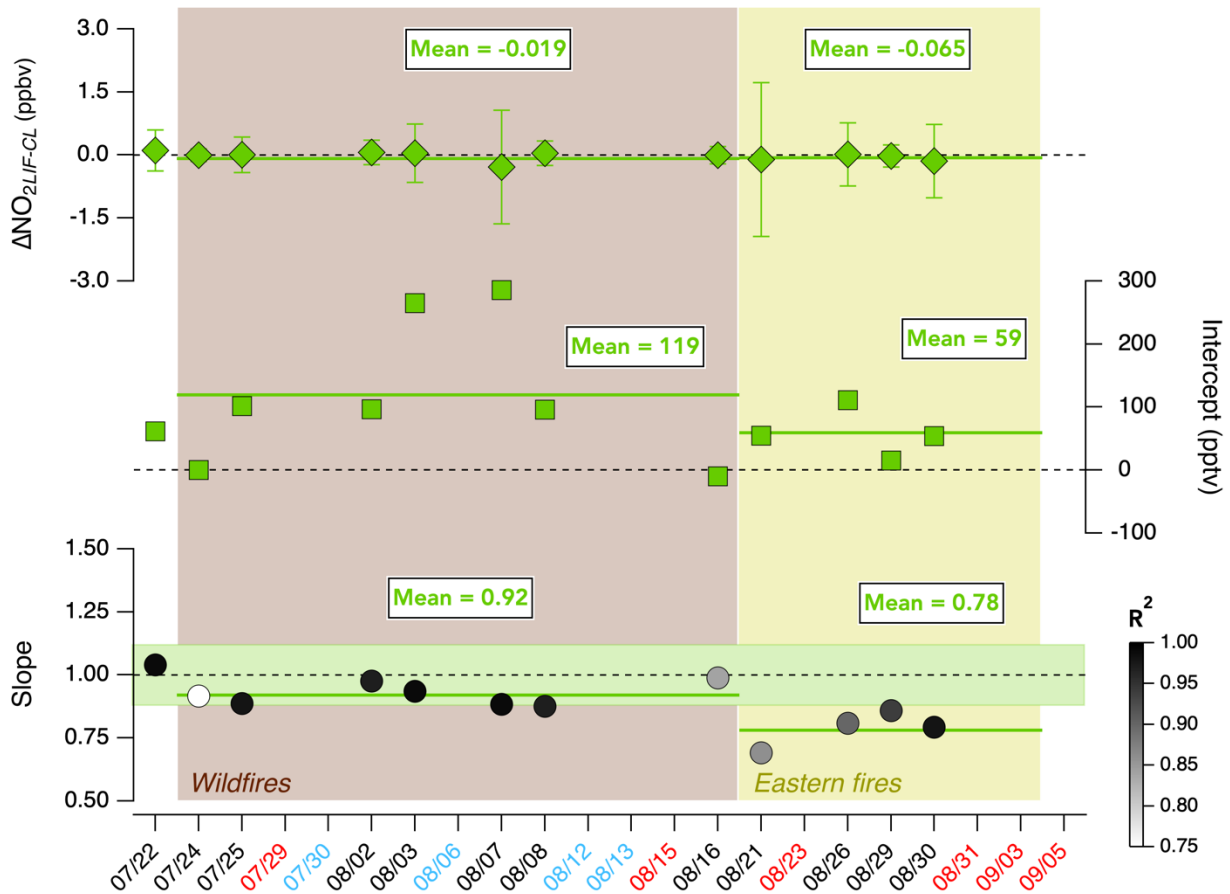


Figure S11 Individual flight comparison of 1Hz NO_2 measurements by LIF versus CL. Slopes (circles) are reported in the bottom panel and colored by the correlation coefficient value as indicated by the color scale. Intercepts (green squares) are reported in the middle panel, and mean $\Delta\text{NO}_{\text{LIF-CL}}$ (green diamonds) values are reported in the top panel. The solid green lines correspond to the average values of each parameter across all wildfire (brown shaded area) and eastern fire (yellow shaded area) flights. The black dotted lines show the zero. The green shaded area in the bottom panel indicates the propagated analytical uncertainty. Flight dates in red indicate that at least one instrument did not report data for those flights. Flight dates in blue indicate that NO_2 mixing ratios were too low to be precisely detected by at least one of the instruments.

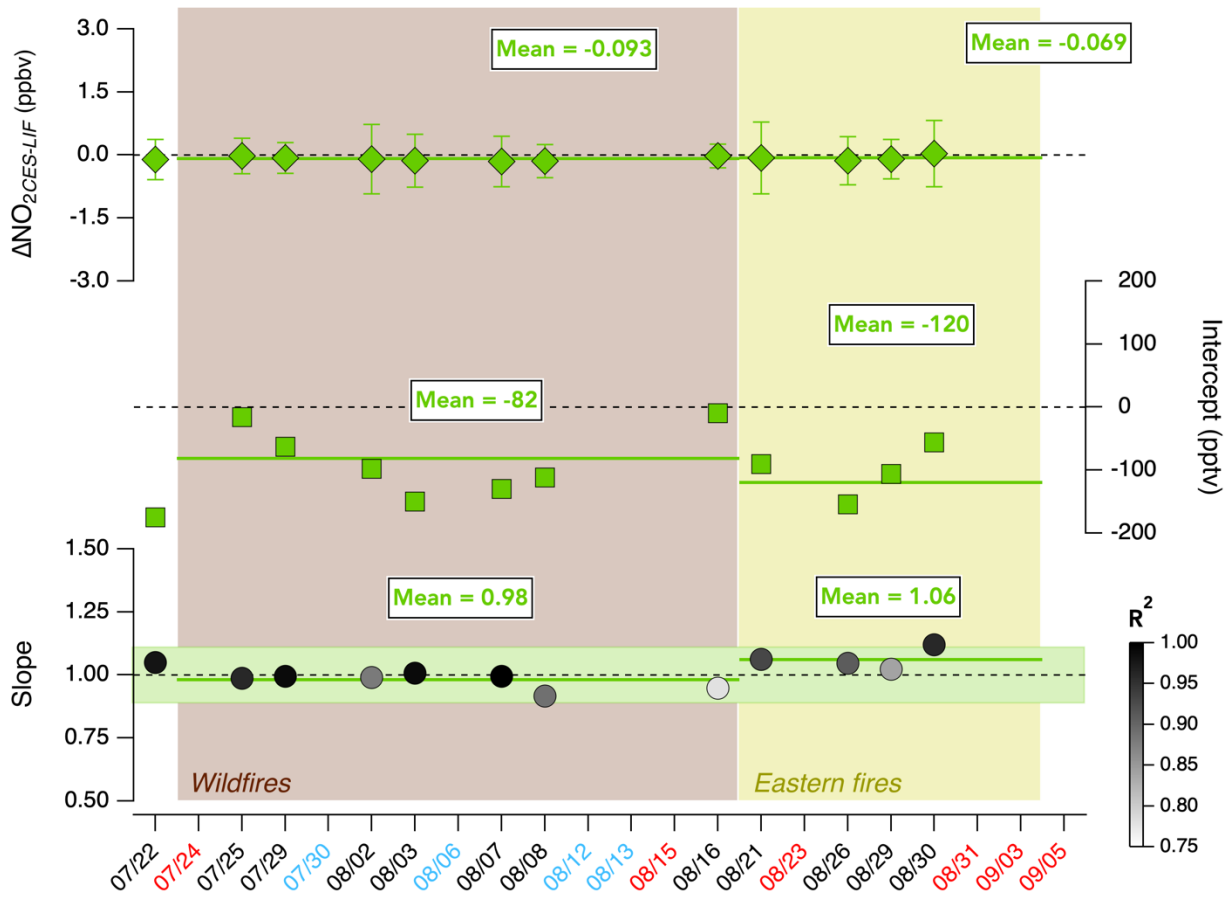


Figure S12 Same as Figure S10 but comparing the CES against the LIF NO_2 measurements.

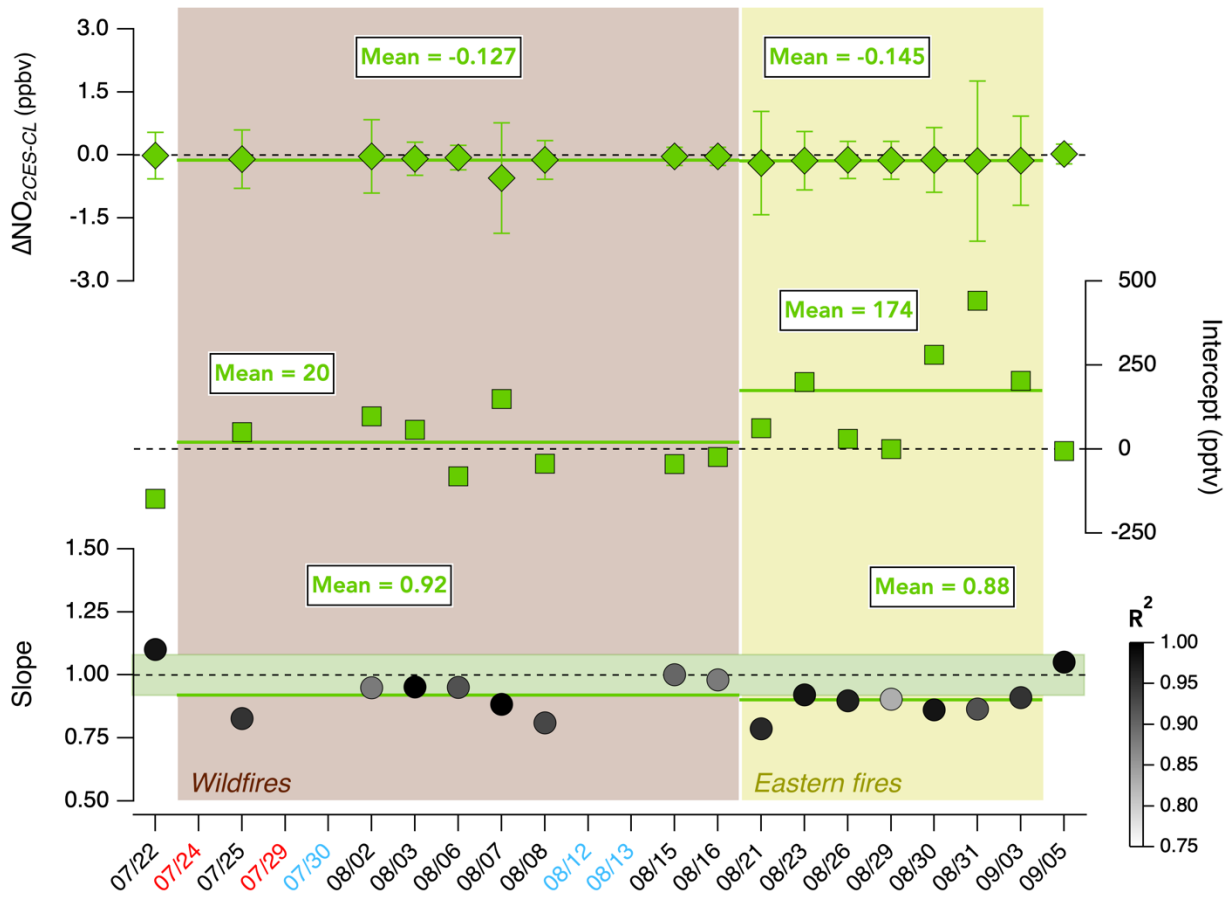


Figure S13 Same as Figure S10 but comparing the CES against the CL NO₂ measurements.

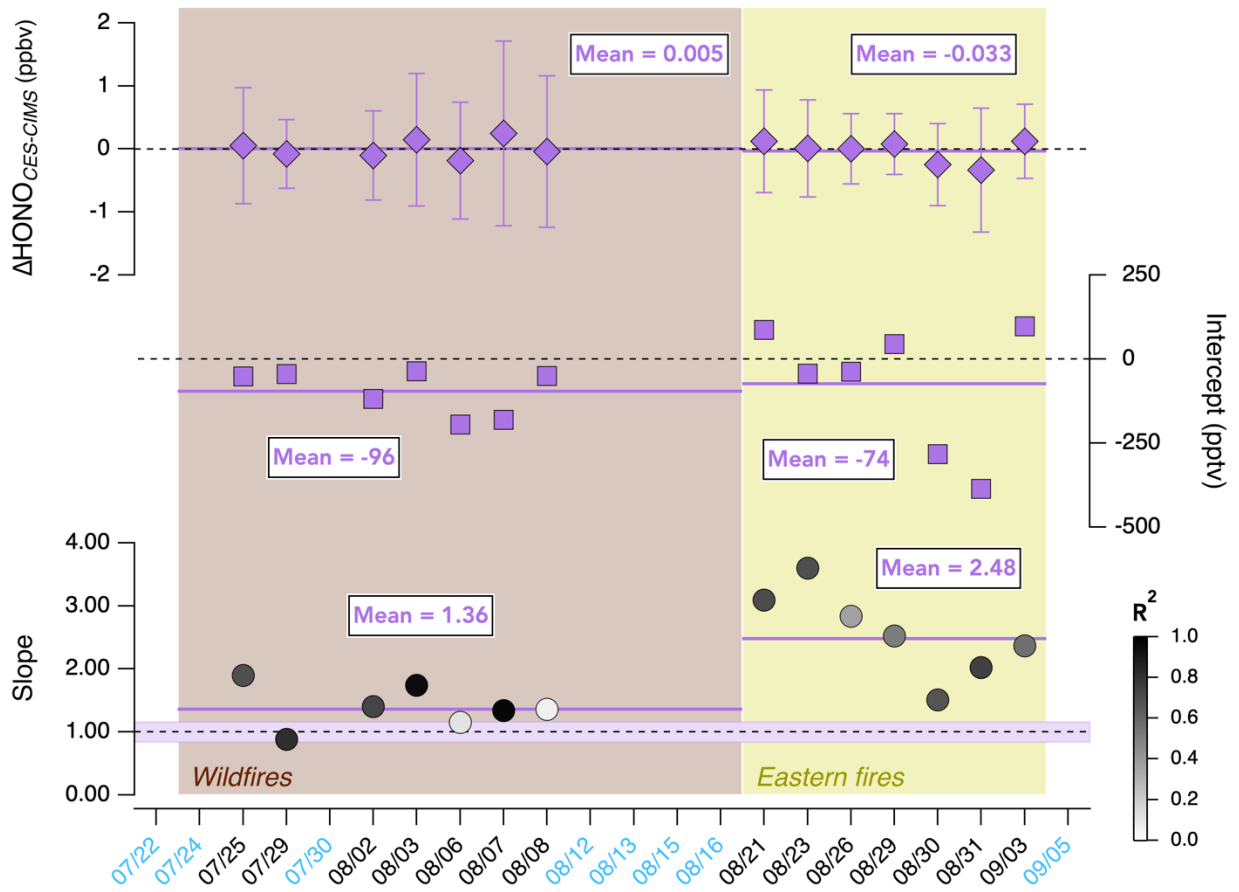


Figure S14 Same as Figure S10 but comparing HONO measurements by CES versus CIMS.

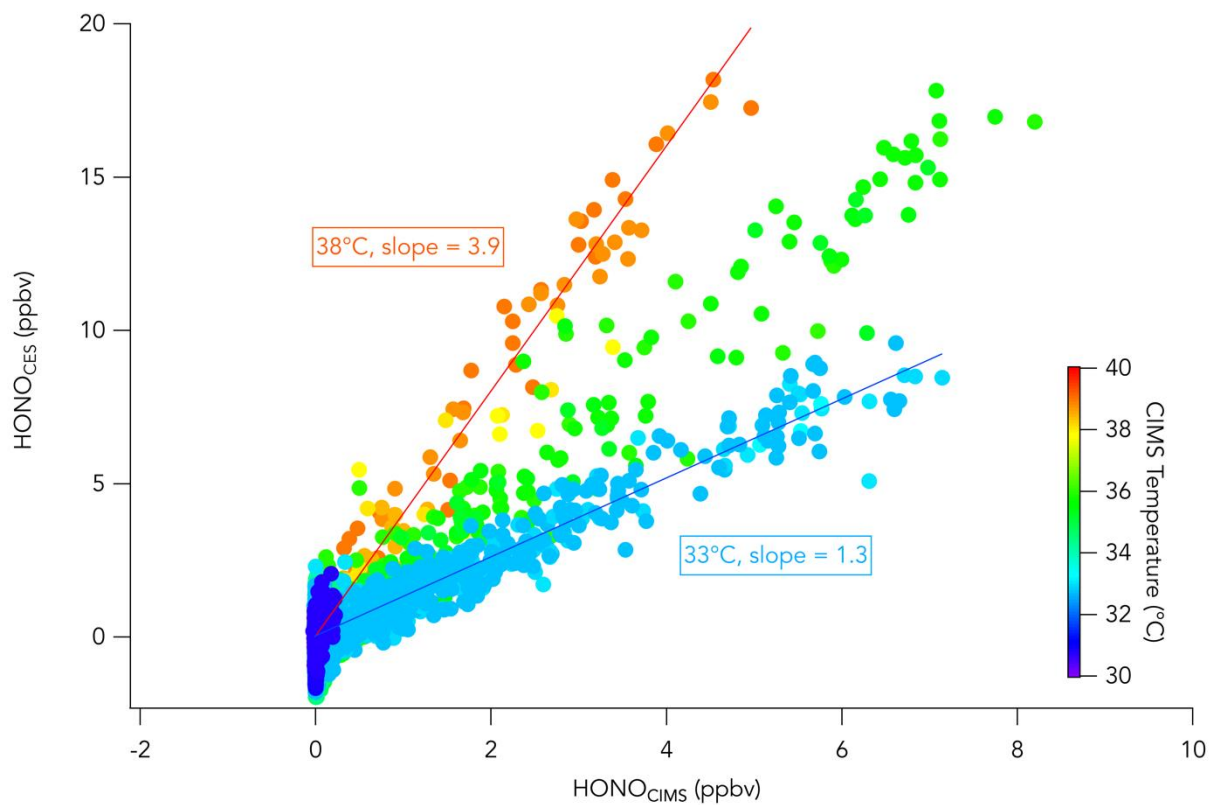


Figure S15 The temperature sensitivity of the CIMS HONO measurement is illustrated by increasing slopes between CES HONO and CIMS HONO with increasing temperatures when sampling wildfire smoke on 25/07/2019. The CIMS temperature was monitored throughout FIREX-AQ.

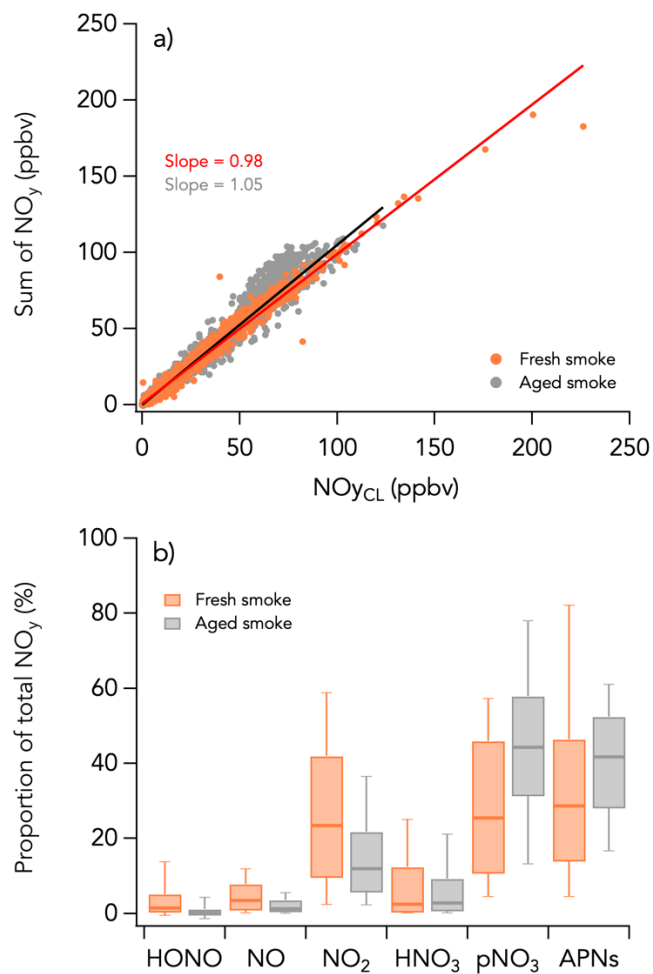


Figure S16 The sum of individually measured NO_y species ($= \text{NO}_x + \text{HONO} + \text{HNO}_3 + \text{APNs} + \text{pNO}_3$) is compared with the total NO_y measurement by CL in fresh (<1h since emission; in red) and aged smoke (<1h since emission; in grey) during the wildfires sampling period in panel a). The black (red) line is the ODR fit in the aged (fresh) smoke. The proportion of individual NO_y species to total NO_y for each type of smoke is given in panel b).

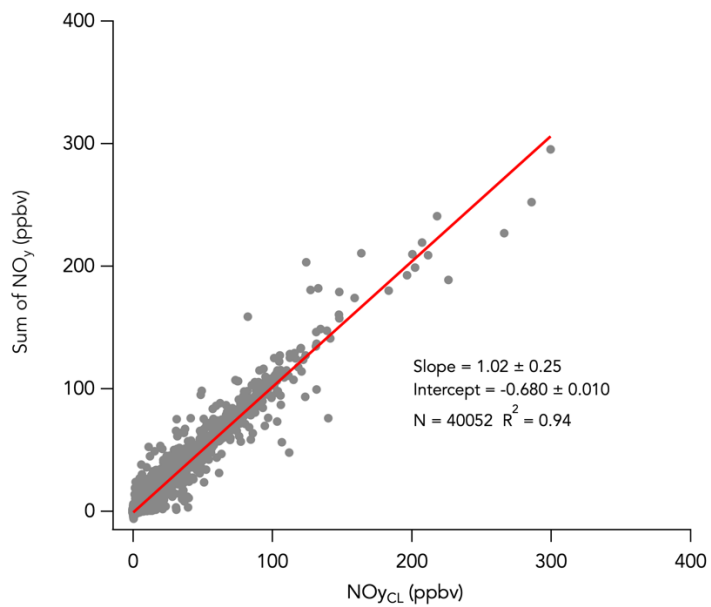


Figure S17 Comparison of the sum of individually measured NO_y species (= NO_x + HONO + HNO₃ + APNs + pNO₃ + alkene hydroxy nitrates + CH₃NO₂ + ClNO₂ + N₂O₅) with the total NO_y measurement by CL. Data from the entire campaign is presented. Here LIF NO, CES HONO and CES NO₂ are used in the sum of NO_y.

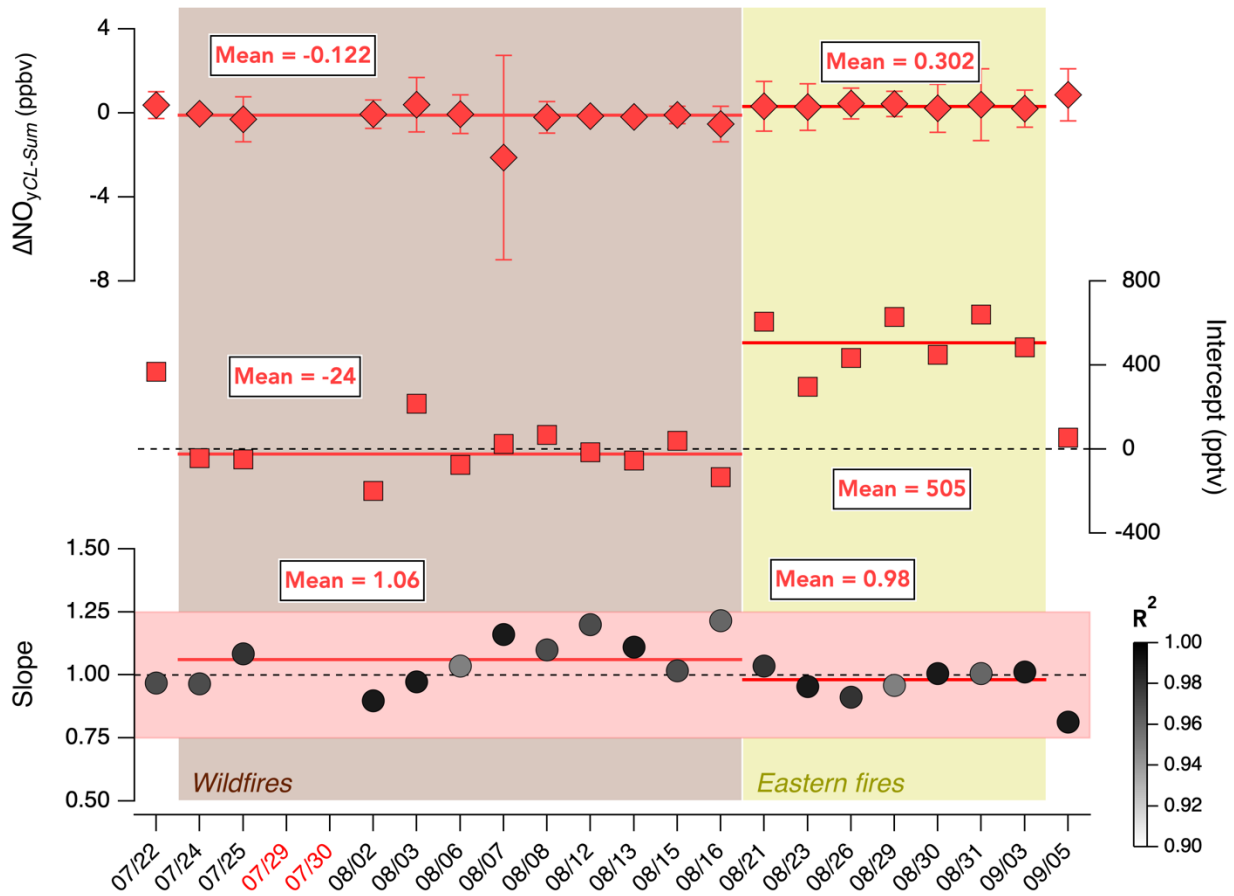


Figure S18 Same as Figure S10 but comparing the sum of individually measured NO_y species (= $\text{NO}_x + \text{HONO} + \text{HNO}_3 + \text{APNs} + \text{pNO}_3$) against the total NO_y measurement by CL.

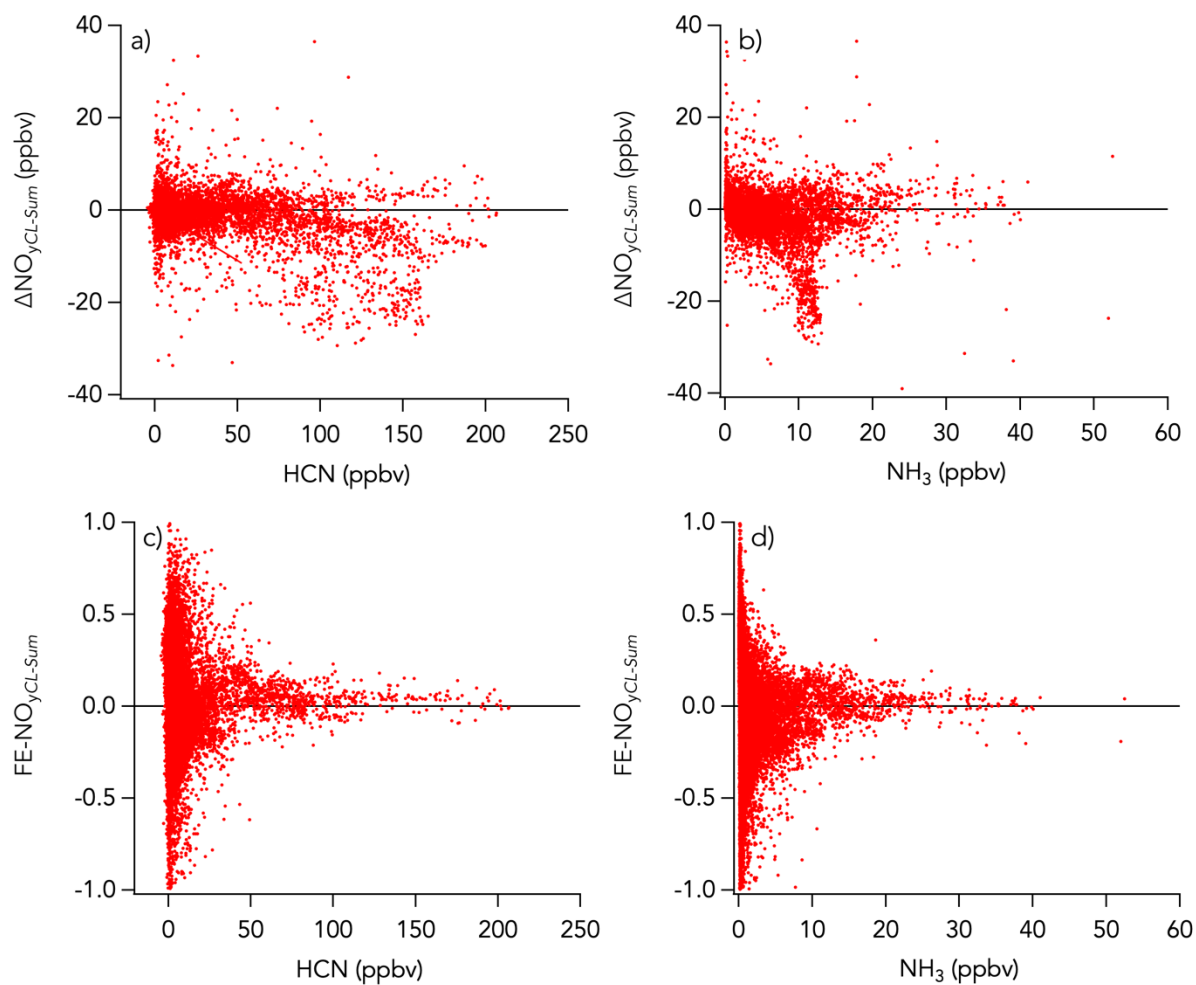


Figure S19 The top two panels show the measurement difference (1 s data) between measured NO_y and the sum of individually measured NO_y species (= $\text{NO}_x + \text{HONO} + \text{HNO}_3 + \text{APNs} + \text{pNO}_3$) as a function of a) HCN and b) NH_3 . The bottom two panels show the fractional error (FE) of 1 s measurements of NO_y as a function of c) HCN and d) NH_3 . Data shown here are for all air masses sampled in fire smoke. HCN was measured by CIMS (Crouse et al., 2009, 2006). NH_3 was measured by PTR-MS (Norman et al., 2007).

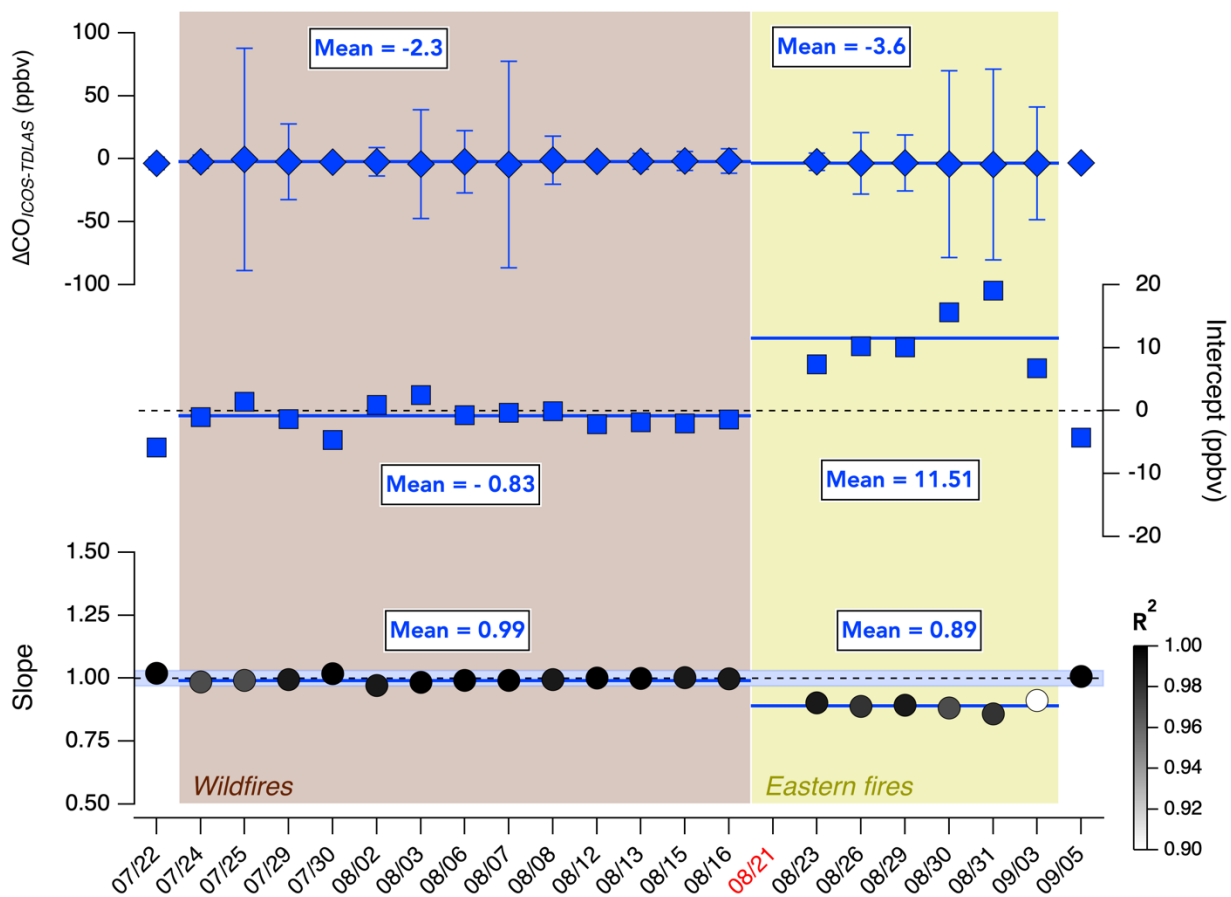


Figure S20 Same as Figure S10 but comparing CO measurements by TDLAS versus ICOS.